

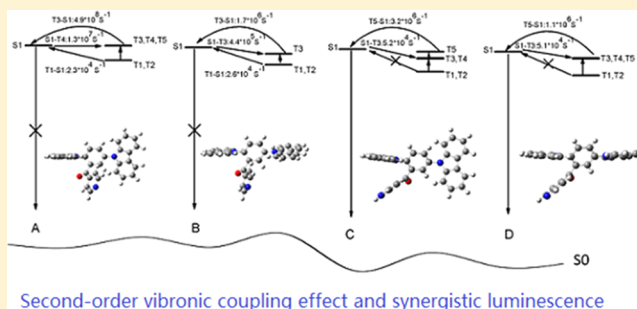
# Electroluminescent Mechanism of Thermally Activated Delayed Fluorescence Emitters: Conformational Effect

Lili Lin,<sup>\*,†</sup> Lei Cai,<sup>†</sup> Jianzhong Fan, and Chuan-Kui Wang<sup>\*</sup>

Shandong Province Key Laboratory of Medical Physics and Image Processing Technology, School of Physics and Electronics, Shandong Normal University, 250014 Jinan, China

## Supporting Information

**ABSTRACT:** Recently, great progress has been made for the thermally activated delayed fluorescence (TADF) molecules. However, the electroluminescent mechanisms of TADF molecules are still not clear enough, which also impedes the development of TADF molecular materials. In this work, the electroluminescent mechanism of the TADF molecule 2,5-di((9*H*-carbazol-9-yl)phenyl)(pyridin-4-yl)methanone (DCBPy) is studied theoretically. Four stable conformers (A, B, C, and D) are found for the DCBPy molecule based on first-principles calculation. The decay rates of excited states for all the four conformers are calculated using the thermal vibrational correlation function method. It is found that conformers A and B are higher in energy than conformers C and D (with significant intramolecular interaction), so conformers C and D are the dominant configurations based on Boltzmann distribution analysis. The emission wavelengths of C and D, which are in good agreement with experimental values, are blue-shift than those of A and B. The calculated fluorescent efficiencies of C and D are 4.2 and 3.7%, respectively, which also agree well with the experimental values. Theoretical study indicates that the prompt emission of the DCBPy molecule is mainly contributed by conformers C and D. The delayed fluorescence of the DCBPy molecule may come from the second-order vibronic coupling effect and also may be contributed by the synergistic effect of conformers A and B that act as exciton collectors. Our theoretical study explains the electroluminescent mechanism of the DCBPy molecule, and the structure–property relationship is also revealed, which could provide help for the effective design of TADF emitters.



## 1. INTRODUCTION

Thermally activated delay fluorescence (TADF) molecules, which can obtain 100% exciton utilization efficiency, have attracted the great attention of both experimental and theoretical workers recently. More than 400 kinds of TADF molecules have been reported, and most of them are composed of donor (D) groups and acceptor (A) groups.<sup>1–7</sup> Nevertheless, the blue and red TADF emitters are still quite limited. One of the reasons is that the electroluminescent mechanism is not clear enough for TADF molecules. Although theoretical studies have given some insights on the TADF mechanisms, it is found that the TADF mechanisms are quite system dependent. Both species and amounts of D and A groups as well as their connection patterns in TADF molecules have great effect on the photophysical properties.<sup>8–13</sup> Nevertheless, the isomerization effect on the photophysical properties of TADF molecules was less studied until now.<sup>14,15</sup> Recently, some regioisomers with TADF were studied, and it was found that one isomer showed DF, but the other one had no DF.<sup>16,17</sup> In the study above, the isomers are induced by different connectivities between D and A groups. In this study, we will focus on one molecule with different conformers to study the influence of relative orientations between D and A groups on

the photophysical properties of TADF molecules. The D–A–D-type 2,5-di((9*H*-carbazol-9-yl)phenyl)(pyridin-4-yl)-methanone (DCBPy) molecule (see Scheme S1), which was reported by Cheng's group recently, will be studied based on first-principles calculations.<sup>18</sup> The excited-state dynamics of the DCBPy molecule will also be studied using the thermal vibrational correlation function (TVCF) method. Our results will explain the electroluminescent mechanism of the DCBPy molecule and help one better understand the structure–property relationship of TADF molecules. The results could also provide some insights on the effective design of TADF emitters.

## 2. THEORETICAL METHODS AND COMPUTATIONAL APPROACH

To study the photophysical properties of D–A–D-type TADF molecules, the excited states have to be studied first using the time-dependent density functional theory (TD-DFT). Since the excited states of D–A–D-type molecules often have

Received: May 28, 2018

Revised: August 7, 2018

Published: August 8, 2018



significant charge transfer (CT) character, the properties of excited states are quite sensitive to the functional adopted. The functionals are tested first (see Table S1). Comparing the calculated absorption and emission wavelengths of DCBPY with experimental values, we found that the PBE0-1/3 functional is more suitable to study this system. Actually, the PBE0-1/3 functional has shown better performance than expected in some other organic systems.<sup>19</sup> Following that, the geometries of the DCBPY molecule in the ground state (S0), the first singlet excited state (S1), and the first triplet excited state (T1) are optimized with PBE0-1/3 functional and 6-31G\* basis set. Unexpectedly, four stable conformers are obtained for DCBPY molecules (shown in Figure 1). The effect of four conformers on the photophysical properties will be studied in detail.

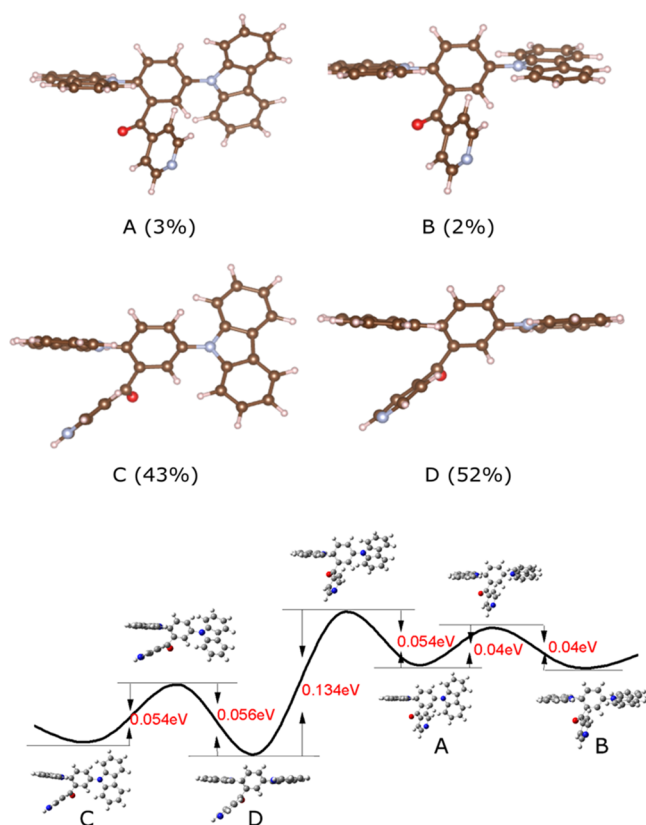


**Figure 1.** Four conformers of the DCBPY molecule and the proportion of each conformer. The energy barriers between four conformers are shown in the lower part.

The geometry optimization of the molecule in S0 is performed using the density functional theory (DFT), while the geometries of excited states are obtained with the TD-DFT method. The UltraFine integration grid and the default Tight SCF procedure are used in our calculation. In optimization, the maximum force is set as 0.00045, and the root mean square (RMS) of the force is 0.00030. The maximum displacement is 0.0018, and RMS displacement is 0.0012. Vibrational information of both S0 and excited states are also obtained by the corresponding methods. In all the calculations above, the PBE0-1/3 functional is used, and the 6-31G\* based set is adopted. All the calculations above are realized in Gaussian 16 program.<sup>20</sup> To obtain the fluorescent efficiency ( $\Phi_{PF}$ ) theoretically, the decay rates of excited states have to be

calculated. The  $\Phi_{PF}$  can be computed by the equation  $\Phi_{PF} = \frac{k_r}{k_r + k_{nr} + k_{ISC}}$ . The  $k_r$  is the radiation rate, which can be calculated by the Einstein spontaneous emission equation as follows:

$$k_r = \frac{f \Delta E_{fi}^2}{1.499} \quad (1)$$

where  $f$  is oscillator strength and  $\Delta E_{fi}$  is the vertical emission energy with the unit of wavenumber ( $\text{cm}^{-1}$ ). The  $k_{nr}$  is the nonradiative rate, which can be deduced based on the first-order perturbation theory and Fermi's golden rule, and it can be written as

$$k_{nr} = \frac{2\pi}{\hbar^2} \sum_{u,v} P_{iv} |H_{fu,iv}|^2 \delta(E_{iv} - E_{fu}) \quad (2)$$

The delta function  $\delta$  is to keep the conservation of energy.  $H$  is the interaction between two different Born–Oppenheimer states, and it contains two components

$$\hat{H}\Psi_{iv} = \hat{H}^{BO}\Phi_i(r, Q)\Phi_v(Q) + \hat{H}^{SO}\Phi_i(r, Q)\Phi_v(Q) \quad (3)$$

with  $\hat{H}^{BO}$  being the nonadiabatic coupling and  $\hat{H}^{SO}$  being the spin–orbit coupling (SOC). The nonradiative decay rate from S1 to S0 can be written as

$$k_{nr} = \frac{2\pi}{\hbar} \sum_{kl} R_{kl} Z_i^{-1} \sum_{vu} e^{-\beta E_{iv}} \langle \Theta_{fu} | \hat{p}_{fk} | \Theta_{iv} \rangle \langle \Theta_{iv} | \hat{p}_{il} | \Theta_{fu} \rangle \delta(E_{iv} - E_{fu}) \quad (4)$$

Here,  $R_{kl} = \langle \Phi_i | \hat{p}_{fk} | \Phi_i \rangle \langle \Phi_i | \hat{p}_{il} | \Phi_i \rangle$  is the nonadiabatic electronic coupling.  $\hat{p}_{fk} = -i\hbar \frac{\partial}{\partial Q_{fk}}$  represents the normal momentum operator of the  $k$ th normal mode in the final electronic state.  $Z_i$  is the partition function. Based on the Franck–Condon principle and applying the Fourier transform of the delta function, the equation can be written as

$$k_{nr} = \sum_{kl} \frac{1}{\hbar^2} R_{kl} \int_{-\infty}^{\infty} dt [e^{i\omega_{if}t} Z_i^{-1} \rho_{IC}(t, T)] \quad (5)$$

Here,  $\rho_{IC}(t, T)$  is the TVCF. Both the methodology and application of this formalism can be found in Peng's and Shuai's works.<sup>21–25</sup> The intersystem crossing (ISC) rate can be computed using the classical Marcus rate equation.

$$\begin{aligned} k_{ISC} &= \frac{V_{ji}^2}{\hbar} \sqrt{\frac{\pi}{K_B T \lambda}} \exp \left[ -\frac{(\Delta G_{ji} + \lambda)^2}{4\lambda K_B T} \right] \\ &= \frac{V_{ji}^2}{\hbar} \sqrt{\frac{\pi}{K_B T \lambda}} \exp \left[ -\frac{\Delta G^\ddagger}{K_B T} \right] \end{aligned} \quad (6)$$

Here,  $K_B$  is the Boltzmann constant and  $T$  is the temperature, which is set as 300 K here.  $V_{ji}$  is the spin–orbit coupling between the S1 state and the triplet excited states (Tn), and it is calculated with the quadratic response function method, which can be realized with the Dalton program.<sup>26</sup> In the activation energy  $\left( \Delta G^\ddagger = \frac{(\Delta G_{ji} + \lambda)^2}{4\lambda} \right)$ ,  $\Delta G_{ji}$  is the energy difference between the S1 state and the Tn state, and  $\lambda$  is the reorganization of two states involved, which can be calculated using the adiabatic potential (AP) energy surface

method.<sup>27,28</sup> In calculation of the ISC rate,  $\Delta G_{ij} = E_{S1} - E_{Tn}$  and  $\Delta G_{ij} = E_{Tn} - E_{S1}$  for the reverse ISC (RISC) process.

### 3. RESULTS AND DISCUSSION

**3.1. Geometric Structures and Energy Levels.** As four conformers of the DCBPY molecule are found, the population proportion of each conformer can be calculated based on the Boltzmann distribution (see the [Supporting Information](#)). It is found that the energy of conformer D is the lowest, and conformer C is only about 4.8 meV higher in energy than conformer D (see [Table S2](#)). However, conformers A and B are, respectively, about 73.7 and 83.3 meV higher in energy than conformer D. To ensure the accuracy of the calculation, the other functionals such as B3LYP and CAM-B3LYP with empirical dispersion are adopted to calculate the energy differences (see the table below). It is found that the energy differences between conformer C and conformer D are close to the value calculated with PBE0-1/3, while the energy values of conformers A and B are a little larger. The results further indicate that the main conformers of the DCBPY molecule are conformers C and D, which is in agreement with the conclusion obtained with PBE0-1/3. The population proportions for A and B are much less than C and D. Consequently, conformers C and D should have a dominant effect on the light-emitting properties of DCBPY molecule. Then, the energy barriers between the four conformers are calculated by performing relaxed scanning (see [Figure 1](#)). It is found that the energy barriers between A and B are only 0.04 eV, which means that conformers A and B can easily change to each other at high temperature or even room temperature. The small energy barrier from A to D (0.054 eV) also indicates that conformer A can transform to conformer D. Nevertheless, it is a little difficult for conformer D to transform to conformer A since the energy barrier is as high as 0.134 eV. From the energy calculation, we also find that conformers C and D can easily transform to each other. Based on the analysis above, we deduce that the DCBPY molecule in the ground state is mainly in the conformers C and D.

For conformers A and C, the surfaces of two donor groups are perpendicular to each other, while they are almost in the same surface in conformers B and D. For conformers A and B, the acceptor group keeps away from the donor group in the orthor-position, while it tends to the donor group in the orthor-position in conformers C and D. The different orientations of the acceptor group relative to the donor group in the orthor-position can induce different intramolecular interactions between them. The reduced density gradient (RDG) method can be used to describe intramolecular interaction. One can refer to the [Supporting Information](#) file for details of this method. From [Figure 2](#), we can see that there is significant intramolecular interaction between the acceptor and the donor at orthor-position in conformers C and D, and it is much stronger than that in conformers A and B. It is also obvious that there is no interaction between the acceptor and the donor in the meta-position in conformers C and D. The significant intramolecular interaction between the donor group and the acceptor group may have important influence on the light-emitting properties.<sup>29,30</sup> One should note that no dispersion is included in our calculation since it is unachievable in the PBE0-1/3 functional. For comparison, the functional CAM-B3LYP with long-range interaction and CAM-B3LYP-D3 with dispersion are also adopted to calculate the absorption and emission wavelengths

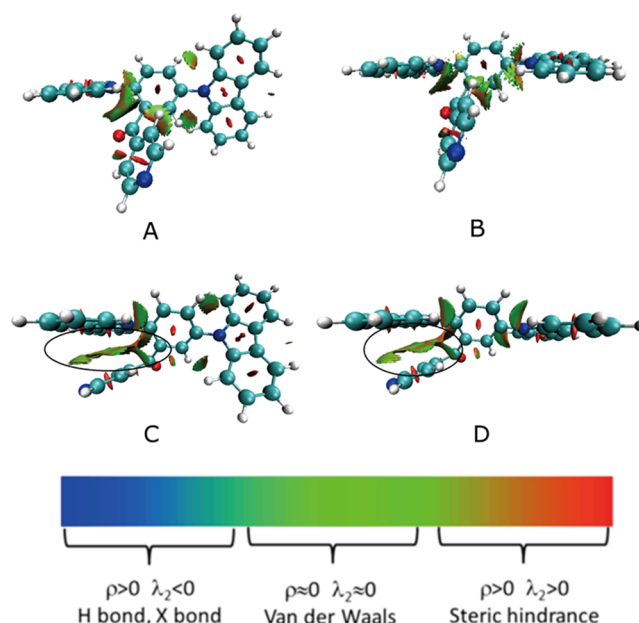


**Figure 2.** Intramolecular interaction between the donor and the acceptor described by the RDG method.

as shown in [Table S1](#). It indicates that the results calculated with CAM-B3LYP and CAM-B3LYP-D3 are almost the same and disagree with the experimental values. It further indicates that the functional PBE0-1/3 is reliable.

**3.2. Properties of Excited States.** The energy levels and electron distribution of the highest occupied molecular orbitals (HOMOs) and the lowest unoccupied molecular orbitals (LUMOs) of the four conformers are shown in [Figure 3](#). It can

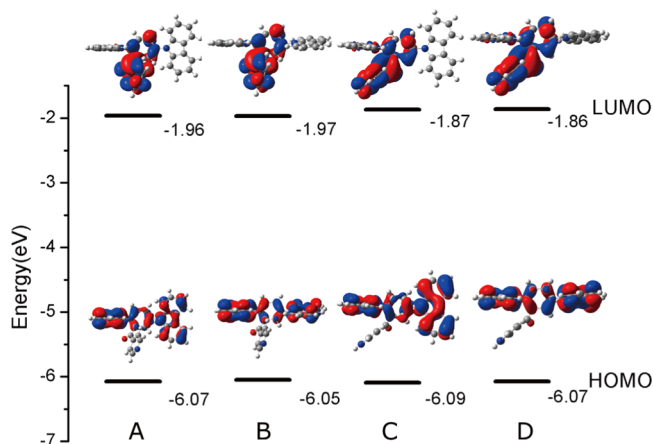


**Figure 3.** Energy and electron distributions of HOMOs and LUMOs for four conformers.

be found that the energies of HOMOs for all the four conformers are almost the same. The energies of LUMOs of conformers C and D are about 0.1 eV higher than those of conformers A and B, which means that the intramolecular interaction can broaden the HOMO–LUMO energy gap. The electron distributions of HOMOs for all the four conformers are quite similar to electrons distributed mainly on the two donor groups. Electrons on LUMOs are only located at the acceptor group for all the four conformers.



The absorption and emission wavelengths of four conformers are also calculated, as shown in Table 1. Both the

**Table 1. Absorption Wavelength, Emission Wavelength, the Oscillator Strength of S1, and the Stoke Shift for Four Conformers<sup>a</sup>**

conformation	absorption (nm)	emission (nm)	<i>f</i>	$\lambda_{\text{shift}}$ (nm)
A	409	577	0.0038	168
B	413	586	0.0044	173
C	391	490	0.0156	99
D	394	502	0.0143	108
exp	400	490		90

<sup>a</sup>Experimental values are listed.

absorption wavelength and emission wavelength of conformers C and D show blue-shift relative to that of conformers A and B. The emission wavelengths of C and D are about 80 nm blue-shift relative to conformers A and B, while there is much weak influence on the absorption wavelength. Smaller Stoke shifts in conformers C and D are also observed. It means that intramolecular interaction can make emission blue-shift and decrease the Stoke shift. It is found that the calculated absorption and emission wavelengths for conformer C are in good agreement with experimental values, and the Stoke shift is only about 9 nm larger than the experimental value. The Stoke shifts calculated for other conformers are much larger. The great discrepancy of conformer A or B comes from the emission wavelengths. It is found that the emission wavelengths for conformers A and B show significant red-shift than experimental values. The absorption wavelengths for conformers A and B agree with the experimental values better. It indicates that there should be large geometric structure relaxation for S1 in conformers A and B after excitation, which can induce larger Stoke shift. The oscillator strengths of conformers C and D are also about 5 times larger than conformers A and B, which predicts stronger emission in conformers C and D.

The adiabatic energy levels of several low-lying excited states are shown in Figure 4. It is found that there are several triplet excited states lying between S1 and T1. For conformers A, C, and D, five triplet states are lower in energy than S1. For conformer B, there are only three triplet states. It is also interesting to find that several triplet excited states are degenerated. The energy gaps between S1 and T1 in conformers A and B are about 0.25 eV, and they become 0.39 eV in conformers C and D.

The transition properties of the low-lying excited states of conformer A and other conformers are also shown in Figures 5 and S1–S3, respectively. From the analysis of natural transition orbitals (NTOs), we can find that all the excited states have both charge transfer (CT) property and the local excited (LE) character. To quantitatively describe the transition properties, the proportions of CT contribution in the excited states are provided (see Figures 5 and S1–S3). The LE proportion in the excited states is calculated based on the overlap between two NTOs involved in the excited states. One can see the detailed information about the calculation of the LE and CT proportions in ref 31. For all the four conformers, the CT proportion for S1 is about 70%, which indicates that all the S1 states for four conformers are CT states. All the other triplet excited states are hybrid local excited and charge transfer states except for T1, T3, and T4 for conformer D with typical LE

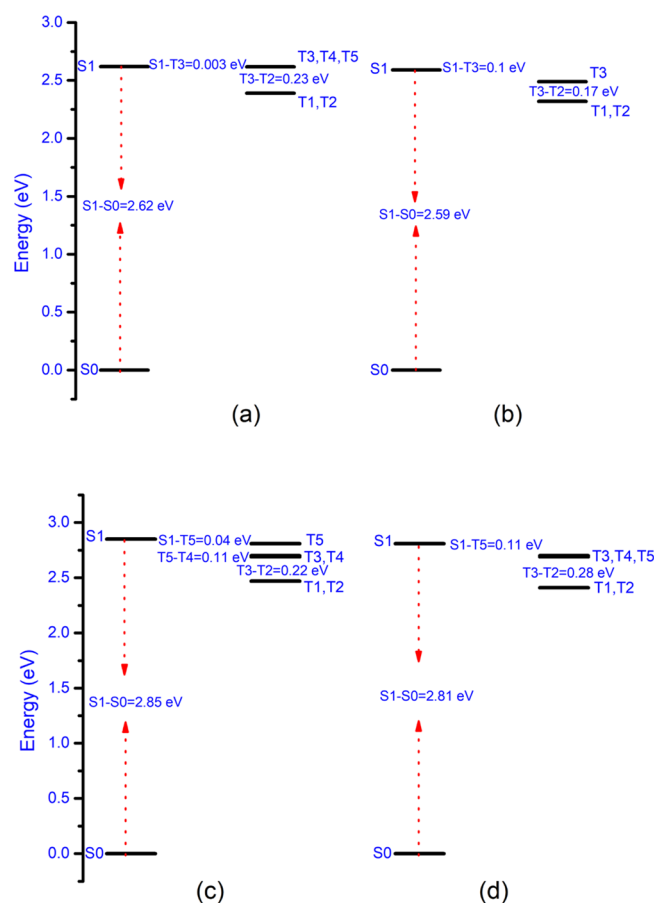


**Figure 4.** Energy levels of several low-lying excited states for A (a), B (b), C (c), and D (d).

characters. The transition properties of excited states may have significant influence on the photophysical properties.

**3.3. Excited-State Dynamics.** Based on the energy structures of excited states for four conformers, the intersystem crossing process should involve several triplet excited states. The spin–orbit coupling (SOC) constants between S1 and the triplet excited states are shown in Table 2. It is found that the SOC values vary significantly for different states. The SOC should have a close relationship with the energy gaps between the S1 state and the triplet state. This variation of SOC may also relate to the transition properties of two excited states.<sup>32–34</sup> The relationships between the SOC and the CT proportion as well as the energy gaps are shown in Figures S4–S6. It is found that there is no linear relationship between the SOC and the CT proportion for all the excited states studied (see Figure S4). The complicated relationship may be induced by complicated influencing factors. To further check the relationship, the energy gap between two states is limited to 0.2–0.3 eV. Nevertheless, it is found that the SOC vs CT proportion shows a reverse relationship for conformers A(B) and C(D) coarsely (Figure S6a,c). The relationship between the SOC and the energy gaps is also complicated (see Figures S5 and S6). Due to the limited systems studied, no similar results are found for the four conformers as that reported by Brédas et al.<sup>35</sup> In addition, we can also find that the SOC values vary from 0.026 to 1.04 cm<sup>−1</sup> for S1–T3, S1–T4, and S1–T5 in conformer A, even though the energy gaps between S1 and three triplet excited states are the same. The variation of SOC cannot be explained only with the CT contribution of triplet

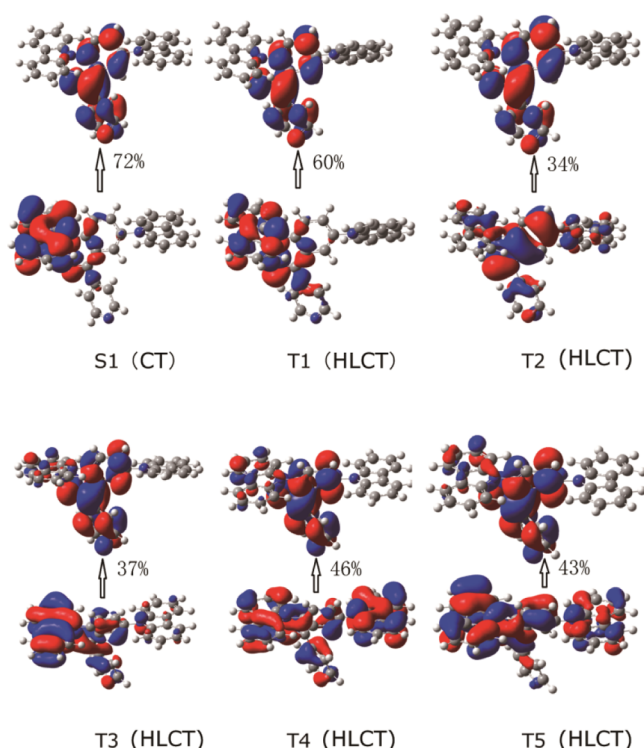


**Figure 5.** Natural transition orbitals (NTOs) for the S1 state and triplet states of conformer A. The CT proportion and transition property for every excited state are also shown.

excited states. Actually, the SOC between S1 and Tn are also related to the geometries. When the SOC is calculated based on the geometries of Tn, the values are quite different from that calculated based on the geometry of S1 (see Table 2). More detailed investigation is needed to reveal the relationship between the SOC and the properties of excited states.

The reorganization energy and the energy differences between S1 and several low-lying triplet excited states for the

four conformers are shown in Table 2. It is found that the reorganization energy varies from 13 to 645 meV. The energy difference between S1 and Tn changes from −3 to −396 meV. All these values combined with the SOC will determine the ISC rates and RISC rates. For conformer A, the ISC rate between S1–T4 is as large as  $10^7 \text{ s}^{-1}$ , while the S1–T1 rate is only  $10^2 \text{ s}^{-1}$ . It indicates the main ISC process should happen between S1 and T4. The S1–T3 intersystem crossing process may also have some contributions due to its considerable quantity of the ISC rate as the S1–T4 process. For conformer B, the ISC rate between S1 and T3 is  $10^5 \text{ s}^{-1}$ , which shows a dominant position in the ISC process. For conformer C, the S1–T3 and S1–T5 ISC processes play important roles in the ISC process. The S1–T3 process in conformer D shows its primary contribution in the ISC process. For simplicity, the effective ISC rate is defined,<sup>36–38</sup> and they are listed in Table 3.

**Table 3.** Radiation Rates, Nonradiative Rates, the Intersystem Crossing Rate, and the Fluorescent Efficiency for the Four Conformers

configuration	$k_r \text{ (s}^{-1}\text{)}$	$k \text{ (s}^{-1}\text{)}$	$k_{\text{ISC}}^{\text{eff}} \text{ (s}^{-1}\text{)}$	$\eta \text{ (\%)}$
A	$7.6 \times 10^5$	$8.9 \times 10^{10}$	$1.16 \times 10^7$	0.0009
B	$8.6 \times 10^5$	$3.2 \times 10^9$	$4.4 \times 10^5$	0.027
C	$4.3 \times 10^6$	$9.7 \times 10^7$	$4.5 \times 10^4$	4.2
D	$3.8 \times 10^6$	$9.8 \times 10^7$	$5.0 \times 10^4$	3.7

It is found that the ISC rates for conformers C and D are much smaller than that of conformers A and B. The fluorescent rates for C and D are about 1 order of magnitude larger than A and B. This is induced by the larger oscillator strength of the S1 states for C and D. The nonradiative rates for C and D are about 3 orders of magnitude smaller than A and B. This can be explained by the reorganization energy analysis. The fluorescent efficiencies for C and D are 4.2 and 3.7%, respectively, while they are quite small for A and B. From our calculation results, we conclude that conformers C and D contribute most to the prompt fluorescence of the molecule.

**Table 2.** Spin–Orbit Coupling (SOC), Reorganization Energy ( $\lambda$ ), Energy Difference ( $G$ ), and the Intersystem Crossing Rates ( $k_{\text{ISC}}$ ) between S1 and Triplet Excited States<sup>a</sup>

configuration		SOC <sup>b</sup> (cm <sup>−1</sup> )	$\lambda$ (meV)	$G$ (meV)	$k_{\text{ISC}}$ (s <sup>−1</sup> )	SOC <sup>c</sup> (cm <sup>−1</sup> )	$k_{\text{RISC}}$ (s <sup>−1</sup> )
A	S1–T1	0.035	104	−231	$6.1 \times 10^2$	1.05	$2.3 \times 10^4$
	S1–T2	0.81	62	−231	$9.6 \times 10^2$	7.4	$8.0 \times 10^4$
	S1–T3	0.27	300	−3	$1.8 \times 10^6$	4.5	$4.9 \times 10^8$
	S1–T4	1.04	361	−3	$1.3 \times 10^7$	1.1	$1.4 \times 10^7$
	S1–T5	0.026	450	−3	$3.2 \times 10^3$	0.12	$7.1 \times 10^4$
B	S1–T1	0.19	406	−268	$2.94 \times 10^2$	1.9	$2.6 \times 10^4$
	S1–T2	0.60	307	−268	$4.8 \times 10^3$	4.9	$4.2 \times 10^5$
	S1–T3	1.0	472	−100	$4.4 \times 10^5$	1.96	$1.7 \times 10^6$
C	S1–T1	0.34	506	−380	$1.1 \times 10$	0.3	9.1
	S1–T2	0.36	334	−380	$2.0 \times 10$	0.8	$1.2 \times 10^2$
	S1–T3	0.77	484	−160	$5.2 \times 10^4$	0.13	$1.6 \times 10^3$
	S1–T4	0.052	399	−152	$6.9 \times 10^2$	0.15	$5.4 \times 10^3$
	S1–T5	0.0069	13	−42	$1.0 \times 10^4$	0.12	$3.2 \times 10^6$
D	S1–T1	0.26	481	−396	4.3	0.62	$2.4 \times 10$
	S1–T2	0.30	155	−396	0	1.6	8.8
	S1–T3	1.03	645	−119	$5.1 \times 10^4$	0.19	$1.8 \times 10^3$
	S1–T4	0.031	356	−119	$8.5 \times 10^2$	1.1	$1.1 \times 10^6$
	S1–T5	0.022	467	−113	$1.6 \times 10^2$	0.75	$2.0 \times 10^5$

<sup>a</sup>The reverse ISC (RISC) rates ( $k_{\text{RISC}}$ ) are also listed.  $k_{\text{ISC}}$  and  $k_{\text{RISC}}$  are calculated based on SOC<sup>b</sup> and SOC<sup>c</sup> values, respectively. <sup>b</sup>SOC between S1 and Tn calculated based on the geometry of S1. <sup>c</sup>SOC between S1 and Tn calculated based on the geometry of Tn.

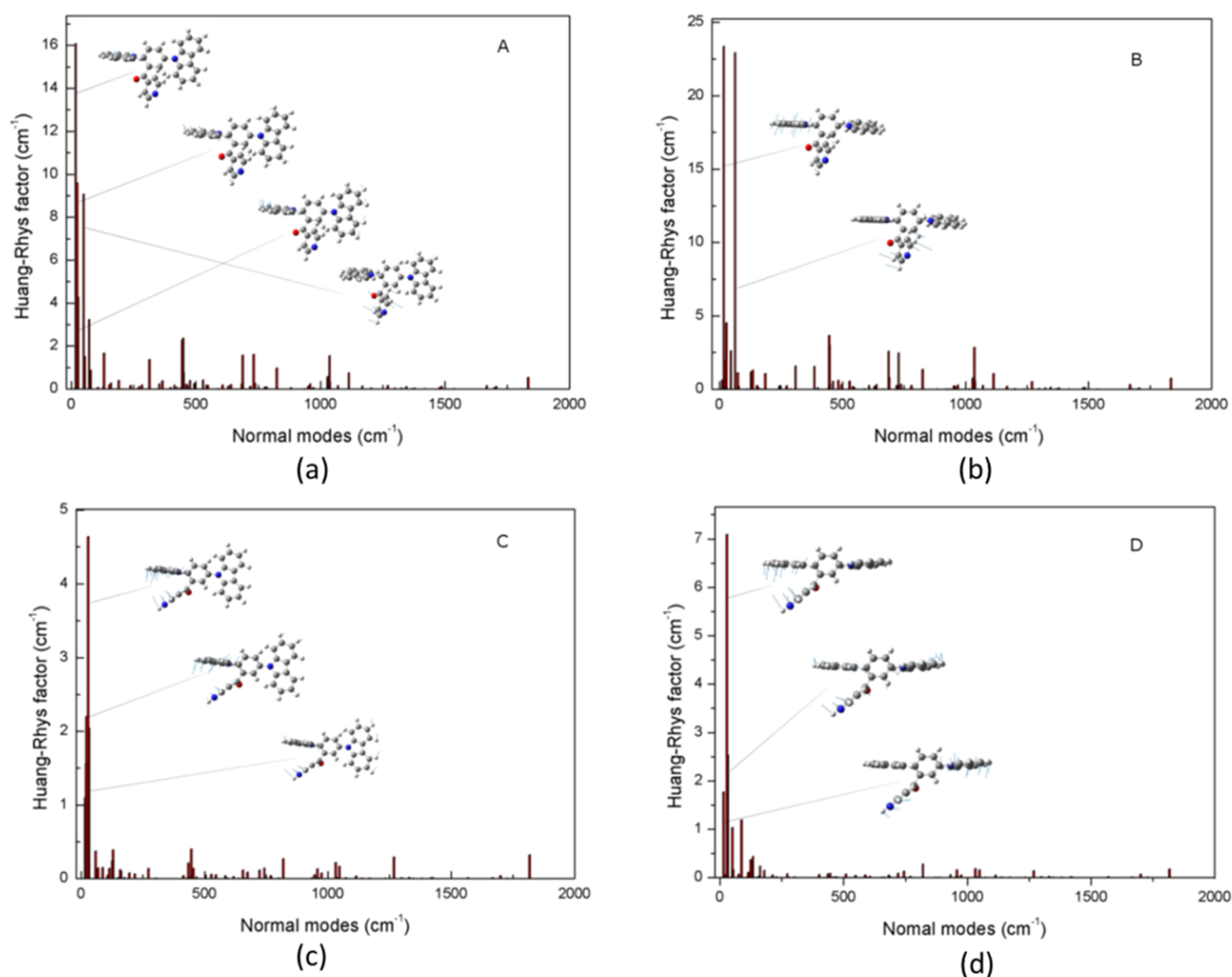


**Figure 6.** Huang–Rhys factors between S1 and S0 for every vibrational mode of the four conformers.

The nonradiative rate of S1 has a close relationship with the reorganization energy and Huang–Rhys factors between S1 and S0. The reorganization energy ( $\lambda$ ) can be expressed as a sum of the contributions from normal mode analysis in the harmonic oscillator approximation

$$\lambda_{\text{gs}} = \sum_{k \in \text{gs}} \lambda_k = \sum_{k \in \text{gs}} \hbar \omega_k \text{HR}_k \quad (7)$$

$$\lambda_{\text{es}} = \sum_{k \in \text{es}} \lambda_k = \sum_{k \in \text{es}} \hbar \omega_k \text{HR}_k \quad (8)$$

$$\text{HR}_k = \frac{\omega_k D_k^2}{2\hbar} \quad (9)$$

Here,  $\text{HR}_k$  represents the Huang–Rhys factor for the  $k$ th mode and  $D_k$  is the displacement for mode  $k$  between the equilibrium geometries of S0 and S1. In the sum,  $k \in \text{gs}$  means that  $k$  represents the vibration modes in the ground state (gs), and  $k \in \text{es}$  means that  $k$  represents the mode of the excited state (es). All data can be obtained by the DUSHIN module in MOMAP.<sup>39</sup> The HR factors for S1 of the four conformers are depicted in Figure 6. It is found that the HR factors for conformers C and D are much smaller than conformers A and B. The maximum values of the HR factors ( $\text{HR}_{\text{max}}$ ) for A and B (16.08 and 23.35, respectively) are all larger than C and D

(7.04 and 7.09, respectively). By detailed analysis, the vibrational modes in the low-frequency region ( $<150 \text{ cm}^{-1}$ ) mainly come from the out-of-surface vibration of the donor and the acceptor. This kind of vibration modes could be effectively suppressed due to the intramolecular interaction between the donor and the acceptor for C and D, which induces smaller HR factors and also smaller reorganization energy. It is also the main reason that induces smaller nonradiative rates in conformers C and D. Our calculation results indicate that the energy dissipation pathways are effectively quenched by the intramolecular interaction between the donor and the acceptor. This is in accordance with our former studies,<sup>36–38</sup> which indicate that intermolecular interaction can also effectively suppress the nonradiative rate by hindering some vibration modes, which contribute to the nonradiative process.

**3.4. TADF Mechanism.** Based on the calculation results of excited states' decay rates, we find that the fluorescent efficiencies of conformers A and B are much smaller than those of C and D. Nevertheless, the ISC rates for C and D are much smaller than A and B. Due to the small energy gaps in triplet excited states, the internal conversion process from higher Tn to T1 is so fast that the RISC process should only happen between T1 and S1. From Table 2, we can see that the RISC rates between T1 and S1 for conformers A and B are

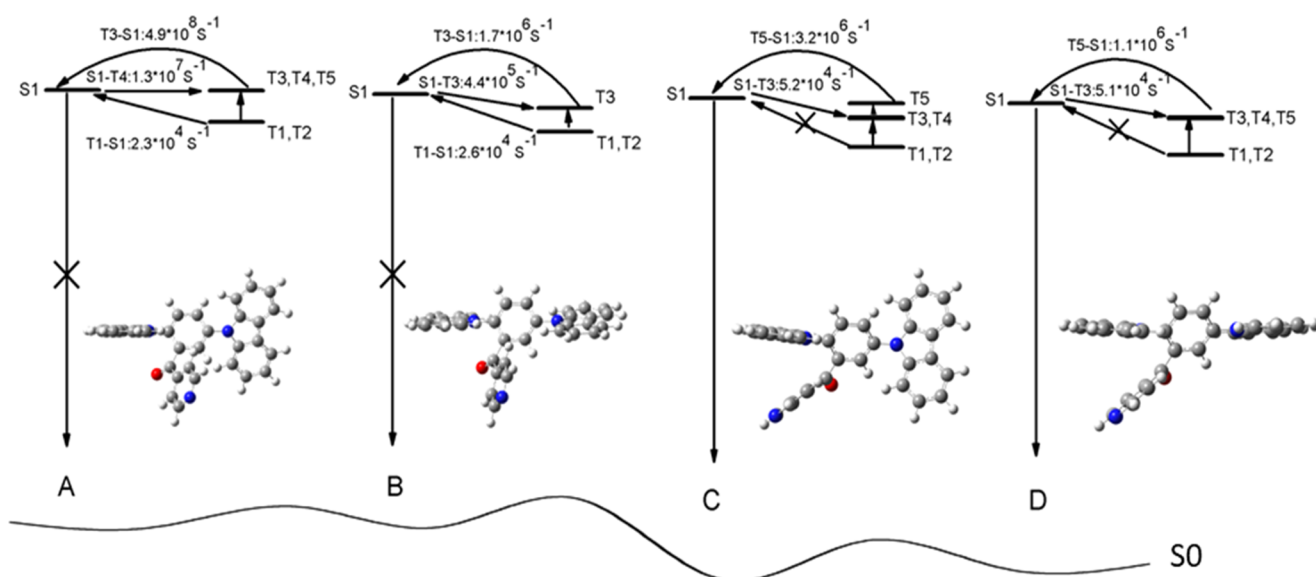


Figure 7. Schematic diagram of the TADF mechanism.

about  $10^4 \text{ s}^{-1}$ , while it is quite small for conformers C and D. It means that the RISC process cannot be realized by upconversion from T1 to S1 in conformers C and D. How was the TADF realized? From the energy of the T1 states for the four conformers, we found that they are quite close in energy for the four conformers (see Table S3). It means that conformers C and D are easily transformed to conformers A and B in the T1 state. Then, the RISC process can be realized in conformers A and B, and the S1 states are obtained. Nevertheless, the nonradiative rates of S1 in conformers A and B are also quite quick, which may induce the decay of the S1 state without fluorescence. Then, the energy of S1 states for four conformers is investigated (see Table S3). It is found that the largest energy difference between all the S1 states is 0.17 eV. It means that there is also another possibility that conformers A and B may transit to conformers C and D in the S1 state. Because of the difficulty to obtain the transition state in excited states, we cannot obtain the energy barrier of excited states of the four conformers. If the energy barrier is not high enough, it is quite possible that conformers A and B may also convert to conformers C and D in S1 states. Then the delayed fluorescence can be observed (see Figure 7). In this mechanism, conformers A and B act as exciton collectors, and conformers C and D are responsible for emission. The synergistic effect of different conformers may contribute to the delayed fluorescence in the DCBPY molecule. Of course, if the high energy barrier between conformers A(B) and C(D) is quite high or if the transform rate is not fast enough in comparison with the nonradiative rate of conformer A(B), the upconversion process will be difficult to realize. Nevertheless, the second-order vibronic coupling effect may work.<sup>40–42</sup> It means that T1 states can upconvert to higher triplet excited states and then transit to the S1 state for conformers C and D. In this mechanism, the conversion among the four conformers in T1 states is disadvantageous to the delayed fluorescence. We should try to cut off the conformer conversion process that happens in T1 states. If both processes can be realized, it will be quite helpful to obtain highly efficient electroluminescence in organic light-emitting diodes (OLEDs).

## 4. CONCLUSIONS

In summary, the electroluminescent mechanism of the DCBPY molecule is investigated based on first-principles study. Four stable conformers are found, with conformers C and D lower in energy than conformers A and B. Significant intramolecular interaction between the acceptor group and the donor group in conformers C and D induce quite different photophysical properties from that in conformers A and B. Our calculation results indicate that the prompt emission of the DCBPY molecule is mainly contributed by conformers C and D. Based on the analysis of the adiabatic energy structure of excited states and the excited-state dynamics, we found that the upconversion processes are complicated. Due to the small RISC rate between S1 and T1 in conformers C and D, the RISC process should be quite difficult. Based on the energy surface of excited states and the decay rates, the delayed fluorescence of the DCBPY molecule may be contributed by the second-order vibronic coupling effect and also the synergistic effect of conformers A and B acting as the exciton collectors and conformers C and D responsible for emission. Our study results indicate that effective modulation of intramolecular interaction between donor groups and acceptor groups may provide effective ways to obtain TADF and highly efficient OLEDs.

## ■ ASSOCIATED CONTENT

### Supporting Information

The Supporting Information is available free of charge on the ACS Publications website at DOI: 10.1021/acs.jpcc.8b05105.

Boltzmann distribution and reduced density gradient methods; schemes of the DCBPY molecule, NTOs, and spin–orbit couplings (PDF)

## ■ AUTHOR INFORMATION

### Corresponding Authors

\*E-mail: linll@sdnu.edu.cn (L.L.).

\*E-mail: ckwang@sdnu.edu.cn (C.K.W.).

### ORCID

Lili Lin: 0000-0002-5319-713X



## Author Contributions

<sup>†</sup>L.L. and L.C. contributed equally to this work.

## Notes

The authors declare no competing financial interest.

## ACKNOWLEDGMENTS

This work was supported by the National Natural Science Foundation of China (Grant Nos 11374195 and 21403133). Thanks to the support of Taishan Scholar Project of Shandong Province and the Scientific Research Foundation of Shandong Normal University. Thanks to the support of the Promotive Research Fund for Excellent Young and Middle-aged Scientists of Shandong Province (Grant No. BS2014CL001) and the General Financial Grant from the China Postdoctoral Science Foundation (Grant No. 2014M560571). Great thanks to Prof. Yi Luo and Tian Lu for their helpful suggestions and discussions in the detailed calculations. Thanks to Prof. Yingli Niu and Qian Peng for the usage of MOMAP program.

## REFERENCES

- (1) Uoyama, H.; Goushi, K.; Shizu, K.; Nomura, H.; Adachi, C. Highly Efficient Organic Light-emitting Diodes from Delayed Fluorescence. *Nature* **2012**, *492*, 234–238.
- (2) Sun, W.; Guo, S.; Hu, C.; Fan, J.; Peng, X. Recent Development of Chemosensors Based on Cyanine Platforms. *Chem. Rev.* **2016**, *116*, 7768–7817.
- (3) Xiong, X.; Song, F.; Wang, J.; Zhang, Y.; Xue, Y.; Sun, L.; Jiang, N.; Gao, P.; Tian, L.; Peng, X. Thermally Activated Delayed Fluorescence of Fluorescein Derivative for Time-resolved and Confocal Fluorescence Imaging. *J. Am. Chem. Soc.* **2014**, *136*, 9590–9597.
- (4) Nagata, R.; Nakanotani, H.; Adachi, C. Near-Infrared Electrophosphorescence up to 1.1 microm using a Thermally Activated Delayed Fluorescence Molecule as Triplet Sensitizer. *Adv. Mater.* **2016**, *29*, No. 1604265.
- (5) Lee, J.; Aizawa, N.; Numata, M.; Adachi, C.; Yasuda, T. Versatile Molecular Functionalization for Inhibiting Concentration Quenching of Thermally Activated Delayed Fluorescence. *Adv. Mater.* **2016**, *29*, No. 1604856.
- (6) Cui, L. S.; Nomura, H.; Geng, Y.; Kim, J. U.; Nakanotani, H.; Adachi, C. Controlling Singlet-Triplet Energy Splitting for Deep-Blue Thermally Activated Delayed Fluorescence Emitters. *Angew. Chem., Int. Ed.* **2017**, *129*, 1593–1597.
- (7) Godumala, M.; Choi, S.; Cho, M. J.; Choi, D. H. Thermally Activated Delayed Fluorescence Blue Dopants and Hosts: from The Design Strategy to Organic Light-emitting Diode Applications. *J. Mater. Chem. C* **2016**, *4*, 11355–11381.
- (8) Duan, C.; Li, J.; Han, C.; Ding, D.; Yang, H.; Wei, Y.; Xu, H. Multi-dipolar Chromophores Featuring Phosphine Oxide as Joint Acceptor: A New Strategy Toward High-efficiency Blue Thermally Activated Delayed Fluorescence Dyes. *Chem. Mater.* **2016**, *28*, 5667–5679.
- (9) Fan, J.; Lin, L.; Wang, C. Decreasing the Singlet-triplet Gap for Thermally Activated Delayed Fluorescence Molecules by Structural Modification on The Donor Fragment: First-principles Study. *Chem. Phys. Lett.* **2016**, *652*, 16–21.
- (10) Tanaka, H.; Shizu, K.; Nakanotani, H.; Adachi, C. Twisted Intramolecular Charge Transfer State for Long-wavelength Thermally Activated Delayed Fluorescence. *Chem. Mater.* **2013**, *25*, 3766–3771.
- (11) Nakanotani, H.; Higuchi, T.; Furukawa, T.; Masui, K.; Morimoto, K.; Numata, M.; Tanaka, H.; Sagara, Y.; Yasuda, T.; Adachi, C. High-efficiency Organic Light-emitting Diodes with Fluorescent Emitters. *Nat. Commun.* **2014**, *5*, No. 4016.
- (12) Lin, L.; Wang, Z.; Fan, J.; Wang, C.-K. Theoretical Insights on the Electroluminescent Mechanism of Thermally Activated Delayed Fluorescence Emitters. *Org. Electron.* **2017**, *41*, 17–25.
- (13) Cao, X.; Zhang, D.; Zhang, S.; Tao, Y.; Huang, W. CN-Containing Donor-acceptor-type Small-molecule Materials for Thermally Activated Delayed Fluorescence OLEDs. *J. Mater. Chem. C* **2017**, *5*, 7699–7714.
- (14) Liu, Y.; Zhan, G.; Fang, P.; Liu, Z.; Bian, Z.; Huang, C. Manipulating Organic Triplet Harvesting in Regioisomeric Microcrystals. *J. Mater. Chem. C* **2017**, *5*, 12547–12552.
- (15) Wang, K.; Zheng, C. J.; Liu, W.; Liang, K.; Shi, Y. Z.; Tao, S. L.; Lee, C. S.; Ou, X. M.; Zhang, X. H. Avoiding Energy Loss on TADF Emitters: Controlling the Dual Conformations of D–A Structure Molecules Based on the Pseudoplanar Segments. *Adv. Mater.* **2017**, *29*, No. 1701476.
- (16) Etherington, M. K.; Franchello, F.; Gibson, J.; Northey, T.; Santos, J.; Ward, J. S.; Higginbotham, H. F.; Data, P.; Kurowska, A.; Dos Santos, P. L.; et al. Regio- and Conformational Isomerization Critical to Design of Efficient Thermally-activated Delayed Fluorescence Emitters. *Nat. Commun.* **2017**, *8*, No. 14987.
- (17) Matulaitis, T.; Imbrasas, P.; Kukhta, N. A.; Baronas, P.; Buciūnas, T.; Banevičius, D.; Kazlauskas, K.; Gražulevičius, J. V.; Juršėnas, S. Impact of Donor Substitution Pattern on the TADF Properties in the Carbazolyl-Substituted Triazine Derivatives. *J. Phys. Chem. C* **2017**, *121*, 23618–23625.
- (18) Rajamalli, P.; Senthilkumar, N.; Gandeepan, P.; Huang, P.-Y.; Huang, M.-J.; Ren-Wu, C.-Z.; Yang, C.-Y.; Chiu, M.-J.; Chu, L.-K.; Lin, H.-W.; et al. A New Molecular Design Based on Thermally Activated Delayed Fluorescence for Highly Efficient Organic Light Emitting Diodes. *J. Am. Chem. Soc.* **2016**, *138*, 628–634.
- (19) Alipour, M. Comparison between Hybrid Functionals Free of Adjustable Parameters and Symmetry-Adapted Cluster–Configuration Interaction for Electronically Excited States of Organic Compounds: Td-Pbe0-1/3 Is Better Than Expected. *Theor. Chem. Acc.* **2015**, *134*, 70.
- (20) Frisch, M. J.; Trucks, G. W.; Schlegel, H. B.; Scuseria, G. E.; Robb, M. A.; Cheeseman, J. R.; Scalmani, G.; Barone, V.; Petersson, G. A.; Nakatsuji, H.; et al. *Gaussian 16*, revision A.03, Wallingford, CT, 2016.
- (21) Niu, Y.; Peng, Q.; Deng, C.; Gao, X.; Shuai, Z. Theory of Excited State Decays and Optical Spectra: Application to Polyatomic Molecules. *J. Phys. Chem. A* **2010**, *114*, 7817–7831.
- (22) Niu, Y.; Peng, Q.; Shuai, Z. Promoting-mode Free Formalism for Excited State Radiationless Decay Process with Duschinsky Rotation Effect. *Sci. China, Ser. B: Chem.* **2008**, *51*, 1153–1158.
- (23) Peng, Q.; Niu, Y.; Shi, Q.; Gao, X.; Shuai, Z. Correlation Function Formalism for Triplet Excited State Decay: Combined Spin–orbit and Nonadiabatic Couplings. *J. Chem. Theory Comput.* **2013**, *9*, 1132–1143.
- (24) Peng, Q.; Fan, D.; Duan, R.; Yi, Y.; Niu, Y.; Wang, D.; Shuai, Z. Theoretical Study of Conversion and Decay Processes of Excited Triplet and Singlet States in a Thermally Activated Delayed Fluorescence Molecule. *J. Phys. Chem. C* **2017**, *121*, 13448–13456.
- (25) Zhang, T.; Peng, Q.; Quan, C.; Nie, H.; Niu, Y.; Xie, Y.; Zhao, Z.; Tang, B. Z.; Shuai, Z. Using the Isotope Effect to Probe an Aggregation Induced Emission Mechanism: Theoretical Prediction and Experimental Validation. *Chem. Sci.* **2016**, *7*, 5573–5580.
- (26) Dalton, a Molecular Electronic Structure Program, Release Dalton2011, 2011. <http://daltonprogram.org>.
- (27) Lemaire, V.; da Silva Filho, D. A.; Coropceanu, V.; Lehmann, M.; Geerts, Y.; Piris, J.; Debije, M. G.; van de Craats, A. M.; Senthilkumar, K.; Siebbeles, L. D. A.; Warman, J. M.; et al. Charge Transport Properties in Discotic Liquid Crystals: A Quantum-Chemical Insight into Structure–Property Relationships. *J. Am. Chem. Soc.* **2004**, *126*, 3271–3279.
- (28) Zhang, T.; Jiang, Y.; Niu, Y.; Wang, D.; Peng, Q.; Shuai, Z. Aggregation Effects on the Optical Emission of 1,1,2,3,4,5-Hexaphenylsilole (HPS): A QM/MM Study. *J. Phys. Chem. A* **2014**, *118*, 9094–9104.
- (29) Tsujimoto, H.; Ha, D.-G.; Markopoulos, G.; Chae, H. S.; Baldo, M. A.; Swager, T. M. Thermally Activated Delayed Fluorescence and



Aggregation Induced Emission with Through-space Charge Transfer. *J. Am. Chem. Soc.* **2017**, *139*, 4894–4900.

(30) Cai, L.; Fan, J.; Kong, X.; Lin, L.; Wang, C.-K. Luminescent Properties of Thermally Activated Delayed Fluorescence Molecule with Intramolecular  $\pi$ - $\pi$  Interaction Between Donor and Acceptor. *Chin. Phys. B* **2017**, *26*, No. 118503.

(31) Chen, R.; Tang, Y.; Wan, Y.; Chen, T.; Zheng, C.; Qi, Y.; Cheng, Y.; Huang, W. Promoting Singlet/triplet Exciton Transformation in Organic Optoelectronic Molecules: Role of Excited State Transition Configuration. *Sci. Rep.* **2017**, *7*, No. 6225.

(32) Jansson, E.; Minaev, B.; Schrader, S.; Ågren, H. Time-dependent Density Functional Calculations of Phosphorescence Parameters for Fac-tris (2-phenylpyridine) iridium. *Chem. Phys.* **2007**, *333*, 157–167.

(33) Mazzone, G.; Quartarolo, A. D.; Russo, N. PDT-correlated Photophysical Properties of Thienopyrrole BODIPY Derivatives. Theoretical Insights. *Dyes Pigm.* **2016**, *130*, 9–15.

(34) Ji, S.; Ge, J.; Escudero, D.; Wang, Z.; Zhao, J.; Jacquemin, D. Molecular Structure–intersystem Crossing Relationship of Heavy-atom-free BODIPY Triplet Photosensitizers. *J. Org. Chem.* **2015**, *80*, 5958–5963.

(35) Samanta, P. K.; Kim, D.; Coropceanu, V.; Brédas, J.-L. Up-Conversion Intersystem Crossing Rates in Organic Emitters for Thermally Activated Delayed Fluorescence: Impact of the Nature of Singlet vs Triplet Excited States. *J. Am. Chem. Soc.* **2017**, *139*, 4042–4051.

(36) Fan, J.; Zhang, Y.; Zhou, Y.; Lin, L.-L.; Wang, C.-K. Excited State Properties of a Thermally Activated Delayed Fluorescence Molecule in Solid Phase Studied by Quantum Mechanics/Molecular Mechanics Method. *J. Phys. Chem. C* **2018**, *122*, 2358.

(37) Fan, J.; Cai, L.; Lin, L.; Wang, C.-K. Excited State Dynamics for Hybridized Local and Charge Transfer State Fluorescent Emitters with Aggregation-induced Emission in The Solid Phase: A QM/MM Study. *Phys. Chem. Chem. Phys.* **2017**, *19*, 29872–29897.

(38) Fan, J.; Lin, L.; Wang, C.-K. Excited State Properties of Non-doped Thermally Activated Delayed Fluorescence Emitters with Aggregation-induced Emission: A QM/MM Study. *J. Mater. Chem. C* **2017**, *5*, 8390–8399.

(39) Reimers, J. R. A Practical Method for The Use of Curvilinear Coordinates in Calculations of Normal-mode-projected Displacements and Duschinsky Rotation Matrices for Large Molecules. *J. Chem. Phys.* **2001**, *115*, 9103–9109.

(40) Gibson, J.; Monkman, A. P.; Penfold, T. J. The Importance of Vibronic Coupling for Efficient Reverse Intersystem Crossing in Thermally Activated Delayed Fluorescence Molecules. *ChemPhysChem* **2016**, *17*, 2956–2961.

(41) Penfold, T. J.; Gindensperger, E.; Daniel, C.; Marian, C. M. Spin-Vibronic Mechanism for Intersystem Crossing. *Chem. Rev.* **2018**, *6975*.

(42) Penfold, T.; Dias, F.; Monkman, A. The Theory of Thermally Activated Delayed Fluorescence for Organic Light Emitting Diodes. *Chem. Commun.* **2018**, *54*, 3926–3935.